

# Why have a Unified Predictive Uncertainty? Disentangling it using Deep Split Ensembles

Utkarsh Sarawgi<sup>1</sup>, Wazeer Zulfikar<sup>1</sup>, Rishab Khincha<sup>1, 2</sup>, Pattie Maes<sup>1</sup>

<sup>1</sup>Massachusetts Institute of Technology, USA

<sup>2</sup>BITS Pilani Goa Campus, India

{utkarshs, wazeer, rkhincha, pattie}@mit.edu

## Abstract

Understanding and quantifying uncertainty in black box Neural Networks (NNs) is critical when deployed in real-world settings such as healthcare. Recent works using Bayesian and non-Bayesian methods have shown how a unified predictive uncertainty can be modelled for NNs. Decomposing this uncertainty to disentangle the granular sources of heteroscedasticity in data provides rich information about its underlying causes. We propose a conceptually simple non-Bayesian approach, *deep split ensemble*, to disentangle the predictive uncertainties using a multivariate Gaussian mixture model. The NNs are trained with clusters of input features, for uncertainty estimates per cluster. We evaluate our approach on a series of benchmark regression datasets, while also comparing with unified uncertainty methods. Extensive analyses using dataset shifts and empirical rule highlight our inherently well-calibrated models. Our work further demonstrates its applicability in a multi-modal setting using a benchmark Alzheimer’s dataset and also shows how deep split ensembles can highlight hidden modality-specific biases. The minimal changes required to NNs and the training procedure, and the high flexibility to group features into clusters makes it readily deployable and useful. The source code is available at <https://github.com/wazeerzulfikar/deep-split-ensembles>

## 1 Introduction

Vast developments across a variety of machine learning tasks have led to extensive deployment of neural networks (NNs) in safety-critical applications ranging from medical diagnosis to self-driving cars (LeCun, Bengio, and Hinton 2015). For reliable, fair and aware models in many regression tasks, the point prediction is not sufficient; the uncertainty or the confidence of that prediction must also be estimated by the model. Understanding what a model does not know is critical to using machine learning systems and mitigating plausible biases and risks in decision making (Gal 2016).

Heteroscedasticity can be modelled as the changing variability of the random disturbance in output values given the input features; in other terms, the probabilistic variability introduced by the stochastic data generation processes. A ‘unified’ predictive uncertainty would be a single estimate modelled for all input features together. Multiple probabilistic methods have been proposed to quantify the same. Bayesian approximation techniques such as variational inference (VI)

(Graves 2011; Blundell et al. 2015), expectation propagation (Hernández-Lobato and Adams 2015), dropout-based VI (Kingma, Salimans, and Welling 2015; Gal and Ghahramani 2016), NNs as Gaussian processes (Lee et al. 2017), deterministic VI (Wu et al. 2018), Bayesian model averaging in low-dimensional parameter subspaces (Izmailov et al. 2020), and approximate Bayesian ensembling (Pearce, Leibfried, and Brintrup 2020) have been shown to be quite useful in modelling the uncertainties in NNs. Non-Bayesian approaches (Osband 2016; Lakshminarayanan, Pritzel, and Blundell 2017; Dusenberry et al. 2020; Jain et al. 2020) that involve bootstrapping and ensembling multiple probabilistic NNs have shown performances comparable to Bayesian methods with reduced computational costs and modifications to the training procedure. Ashukha et al. (2020) performed a broad study of ensembling techniques in context of uncertainty estimation. Qiu, Meyerson, and Miikkulainen (2020) proposed a framework using residual estimation with an I/O kernel (RIO) to estimate uncertainty in any pretrained standard NN. Almost all previous works (MacKay 1992; Kay, Titterton et al. 1999; Welling and Teh 2011; Kendall and Gal 2017; Shridhar, Laumann, and Liwicki 2018; Snoek et al. 2019) including the ones above estimate a unified predictive uncertainty. However, a single ‘unified’ uncertainty would fundamentally be unable to distinguish the granular sources of heteroscedasticity in data, which is critical in applications such as healthcare as it can provide rich information about the underlying causes. ‘Disentangled’ predictive uncertainties would be able to separate these tied sources with granular uncertainty estimates.

We propose a conceptually simple non-Bayesian approach, *deep split ensemble*, to disentangle the predictive uncertainties using a multivariate Gaussian mixture model while training NNs with clusters of correlated features. These correlations can be statistical, or based on different input modalities (multi-modal), domain knowledge or user needs. Figure 1 shows application on simple examples using a multi-dimensional toy regression dataset (Section 3.2), highlighting an advantage of modelling disentangled predictive uncertainties over unified uncertainties.

Recent works have shown how NNs are usually overconfident at predicting probability estimates representative of the true likelihood (Guo et al. 2017). One can use the model’s confidence on a target distribution to compare it with its

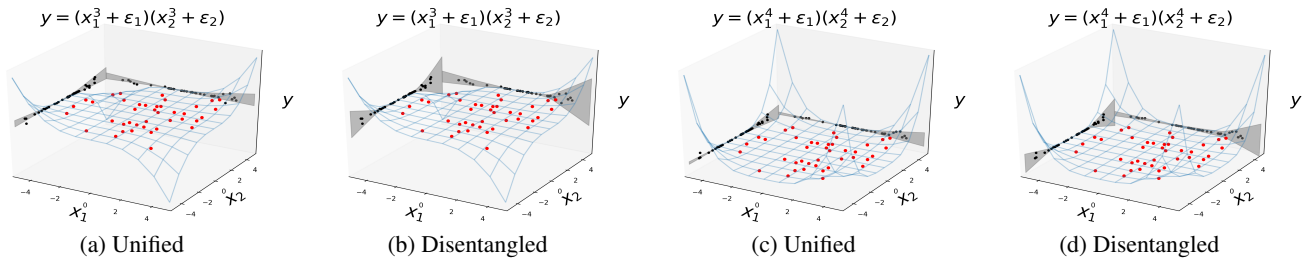


Figure 1: Examples of modelling unified vs disentangled uncertainties on 2 two-dimensional toy regression datasets,  $y = (x_1^3 + \epsilon_1)(x_2^3 + \epsilon_2)$  and  $y = (x_1^4 + \epsilon_1)(x_2^4 + \epsilon_2)$  where  $\epsilon_1, \epsilon_2 \sim \mathcal{N}(0, 3^2)$ . The red points are the observed noisy training samples and the black points are their projections on the respective axes. The grey regions show the predicted mean along with three standard deviations. The disentangled uncertainties have ‘different’ grey regions on the two dimensions (as opposed to unified), and are able to ‘contain’ the black points better. This illustrates how decomposed uncertainties can capture disentangled information about the individual noise in the input features.

accuracy and adjust the predictions (Platt 1999; Guo et al. 2017; Kuleshov, Fenner, and Ermon 2018). However, the distribution over this observed data may shift and eventually be very different once a model is deployed in practice. Robustness of uncertainty estimation under these conditions of distributional shift is necessary for the safe deployment of machine learning systems (Amodei et al. 2016; Varshney and Alemzadeh 2017; Kumar, Liang, and Ma 2019; Thiagarajan et al. 2020). Snoek et al. (2019) recently showed how post-hoc calibration can fail under even a mild shift in the data. We show that modelling disentangled predictive uncertainties using our approach produces inherently well-calibrated estimates per cluster of features, without any post-hoc calibration. We assess it using a granular feature-wise distributional shift. This helps address the critical and practical concerns of risk, uncertainty, and trust in a model’s output.

### Summary of contributions:

1. To our knowledge, we are the first to propose a method to disentangle unified predictive uncertainties with NNs.
2. We perform a rigorous and comprehensive evaluation on the inherent calibration of our models under dataset shifts on benchmark regression datasets.
3. To demonstrate the applicability of our method, we extend it to include domain knowledge, and to a multi-modal setting to highlight the potential hidden modality-specific biases.

## 2 Deep Split Ensembles: Disentangling predictive uncertainties

### 2.1 Notation and setup

Let  $\mathbf{x} \in \mathbb{R}^d$  represent a set of  $d$ -dimensional input features and  $y \in \mathbb{R}$  denote the real-valued label for regression. Given a training dataset  $\mathcal{D} = \{(\mathbf{x}_n, y_n)\}_{n=1}^N$  consisting of  $N$  i.i.d. samples, we model the probabilistic predictive distribution  $p_\theta(y|\mathbf{x})$  using a neural network with parameters  $\theta$ .

We split the set of  $d$  input features of  $\mathbf{x}$  into  $k$  exhaustive clusters,  $k \neq 1$ , each containing  $m_i$  number of features, s.t.  $\forall_{i=1}^k m_i < d$  and  $\sum_{i=1}^k m_i = d$ . Features are

non-overlapping i.e. a particular feature belongs to only one cluster. Let  $\mathbf{c}_n^i \in \mathbb{R}^{m_i}$  denote  $i^{\text{th}}$  cluster containing  $m_i$  input features of  $n^{\text{th}}$  data point  $\mathbf{x}_n$ . Thus,  $\{(\mathbf{c}_n^i, y_n)\}_{n=1}^N$  represents  $i^{\text{th}}$  input feature cluster and corresponding label for  $N$  samples. Label  $y_n$  is the same across any input cluster  $\mathbf{c}_n^i$  corresponding to the  $n^{\text{th}}$  data point (Equation 2). For clusters with one feature each,  $k = d \implies \forall_{i=1}^k m_i = 1$ .

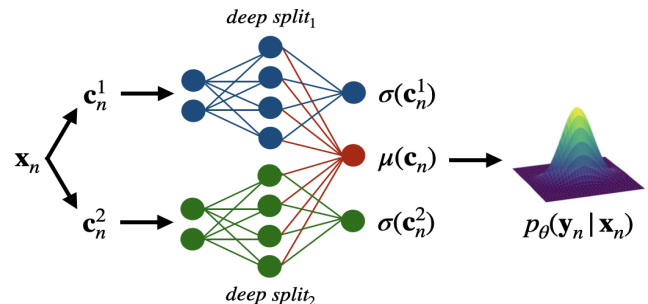


Figure 2: A representative Deep Split NN model architecture

### 2.2 Defining ‘Deep Split Ensemble’ with multivariate Gaussian mixture

Jacobs et al. (1991); Xu, Jordan, and Hinton (1995) showed how local expert networks can be explicitly trained on differing input features and used a gating network to combine into a mixture of experts model. Hinton (1999) introduced the product of experts model in which several individual probabilistic models are combined together to model the data. Williams, Agakov, and Felderhof (2002) further considered each expert as a Gaussian for a richer structure. Recent works have shown improvements in performance of ensembles by training them jointly with a unified loss as compared to post-hoc ensembling of independent models (Lee et al. 2015; Furlanello et al. 2018; Dutt, Pellerin, and Quénot 2020). Such mixture of experts have been widely used to predict the target value only. We model each expert to predict an uncertainty given the corresponding input features, while also contributing to a single target value prediction (Figure 2), trained with a unified loss (Section 2.3). This allows for disentangled predictive

uncertainties per cluster of input features, as opposed to a single unified predictive uncertainty.

Our method forms clusters of input features (Section 2.3), and splits NNs proportionately. Each split, referred to as a ‘deep split’, takes in a cluster of input features  $\mathbf{c}_n^i$  and models its output as the predicted mean  $\mu_\theta(\mathbf{c}_n^i)$  and the standard deviation  $\sigma_\theta(\mathbf{c}_n^i)$  parameterizing a Gaussian distribution. However, only one common mean  $\mu_\theta(\mathbf{c}_n)$  is learnt across the deep splits (Equation 1). This is because while we aim to disentangle the predictive uncertainties, we still want the model to learn the regression value using all the input features together. We combine these Gaussian output distributions of deep splits to parametrize a multivariate Gaussian (MVN)  $p_\theta(\mathbf{y}_n|\mathbf{x}_n)$ ;  $\mathbf{y}_n \sim \mathcal{N}(\boldsymbol{\mu}_\theta(\mathbf{x}_n), \Sigma_\theta(\mathbf{x}_n))$ , using the common mean and the covariance matrix  $\Sigma_\theta(\mathbf{x}_n)$  represented as a diagonal matrix of the  $k$  individual variances (Equations 2 and 3). We call this entire model ‘deep split NN’ (Figure 2).

$$\boldsymbol{\mu}_\theta(\mathbf{x}_n) = [\mu_\theta(\mathbf{c}_n^1), \dots, \mu_\theta(\mathbf{c}_n^k)]^T; \quad \forall_{i=1}^k \mu_\theta(\mathbf{c}_n^i) = \mu_\theta(\mathbf{c}_n) \quad (1)$$

$$\Sigma_\theta(\mathbf{x}_n) = \text{diag}(\sigma_\theta^2(\mathbf{c}_n^1), \dots, \sigma_\theta^2(\mathbf{c}_n^k)) \\ \mathbf{y}_n = [y_n^1, \dots, y_n^k]^T; \quad \forall_{i=1}^k y_n^i = y_n \quad (2)$$

$$p_\theta(\mathbf{y}_n|\mathbf{x}_n) = \frac{1}{\sqrt{(2\pi)^k |\Sigma_\theta(\mathbf{x}_n)|}} \times \\ \exp\left(-\frac{1}{2}(\mathbf{y}_n - \boldsymbol{\mu}_\theta(\mathbf{x}_n))^T \Sigma_\theta(\mathbf{x}_n)^{-1}(\mathbf{y}_n - \boldsymbol{\mu}_\theta(\mathbf{x}_n))\right) \quad (3)$$

The weight update equations of a network modelling a Gaussian output distribution, as derived by Nix and Weigend (1994), show that the learning rate  $\eta$  is affected by variations in  $\sigma^2(\mathbf{x})$ ;  $\eta$  is effectively amplified for input patterns where  $\sigma^2(\mathbf{x})$  is smaller than average compared to patterns where  $\sigma^2(\mathbf{x})$  is larger than average. While this behavior is noted across the datapoints, it is further applicable in our network across deep splits modelling different  $\sigma^2(\mathbf{c}^i)$ , assisting cluster-wise gradient backpropagation through our model. This biases the allocation of the network’s resources towards lower-noise regions, discounting regions of the input space where the network is producing larger than average uncertainties, thus implementing a form of robust regression.

Lakshminarayanan, Pritzel, and Blundell (2017); Snoek et al. (2019); Dusenberry et al. (2020); Dietterich (2000); Pearce, Leibfried, and Brintrup (2020) have shown improved performance with an ensemble of an NN initialized with random parameters, compared to the NN performance. We train a parallel ensemble of our deep split NNs while uniformly weighing the predictions across the ensemble. This forms a mixture of uniformly-weighted multivariate Gaussians.

We call the above method the ‘deep split ensemble’, and train it using a simple procedure.

## 2.3 Training procedure

**Feature clustering and NN splitting:** The input feature space is required to be split into  $k$  exhaustive clusters. For splitting, we use hierarchical clustering based on Pearson correlation distance, since we want to estimate predictive uncertainties for clusters of similar features. The dendograms thus obtained upon hierarchical clustering with complete linkage are thresholded relative to the maximum distance to obtain feature clusters (details in Appendix A.1). Note that we are clustering features, which should not be confused with clustering datapoints. The NN is then split to train using all feature clusters (Section 2.2 and Figure 2). We also show splitting based on domain knowledge (Section 3.4) and across input modalities (Section 3.5).

**Training criterion:** The deep split ensemble is trained with the clusters of input features of all training datapoints and their corresponding ground truth labels using a proper scoring rule  $l(\theta, \mathbf{x}, \mathbf{y})$ . We optimize for the negative log-likelihood (NLL) of the joint distribution  $p_\theta(\mathbf{y}|\mathbf{x})$  according to Equation 4.

$$-\log p_\theta(\mathbf{y}_n|\mathbf{x}_n) = \frac{1}{2}(\log \Sigma_\theta(\mathbf{x})) \\ + (\mathbf{y} - \boldsymbol{\mu}_\theta(\mathbf{x}))^T \Sigma_\theta(\mathbf{x})^{-1}(\mathbf{y} - \boldsymbol{\mu}_\theta(\mathbf{x})) + \text{constant} \quad (4)$$

**Parallel ensembling:** As discussed in Section 2.2, we train a parallel ensemble of our deep split models initialized with random NN parameters, while uniformly weighing the predictions across the ensemble. This forms a mixture of uniformly-weighted multivariate Gaussians  $p_E(\mathbf{y}_n|\mathbf{x}_n)$  as shown in Equation 5, where  $E$  is the total number of models in the ensemble. The mean  $\boldsymbol{\mu}_E(\mathbf{x}_n)$  and variance  $\Sigma_E(\mathbf{x}_n)$  of such a mixture  $E^{-1} \sum_e \mathcal{N}(\boldsymbol{\mu}_{\theta_e(\mathbf{x}_n)}, \Sigma_{\theta_e(\mathbf{x}_n)})$  are shown in Equations 6 and 7 respectively (refer to Appendix B.1 for derivation). For ease of computing quantiles and predictive probabilities, we approximate this ensemble prediction as a Gaussian whose mean and variance are that of the mixture. For a fair comparison with other uncertainty estimation methods that use ensembles of 5 models (Lakshminarayanan, Pritzel, and Blundell 2017; Pearce, Leibfried, and Brintrup 2020), we use a value of  $E = 5$  for our experiments (Section 3). Refer to Appendix D.2 for results with  $E = 1$  and  $E = 10$

$$p_E(\mathbf{y}_n|\mathbf{x}_n) = E^{-1} \sum_{e=1}^E p_{\theta_e}(\mathbf{y}_n|\mathbf{x}_n) \quad (5)$$

$$\boldsymbol{\mu}_E(\mathbf{x}_n) = E^{-1} \sum_{e=1}^E \boldsymbol{\mu}_{\theta_e}(\mathbf{x}_n) \quad (6)$$

$$\Sigma_E(\mathbf{x}_n) = \text{diag}(\sigma_E^2(\mathbf{c}_n^1), \dots, \sigma_E^2(\mathbf{c}_n^k)) \\ \forall_{i=1}^k \sigma_E^2(\mathbf{c}_n^i) = E^{-1} \sum_{e=1}^E (\sigma_{\theta_e}^2(\mathbf{c}_n^i) + \mu_{\theta_e}^2(\mathbf{c}_n^i)) - \mu_E^2(\mathbf{c}_n^i) \quad (7)$$

Datasets	RMSE				NLL			
	RIO	Deep Ensembles	Anchored Ensembling	Deep Split Ensembles	RIO	Deep Ensembles	Anchored Ensembling	Deep Split Ensembles <sup>1</sup>
Boston	–	3.28 ± 1.00	3.09 ± 0.17	<b>2.53 ± 0.15</b>	–	2.41 ± 0.25	2.52 ± 0.05	<b>2.23 ± 0.04</b>
Concrete	5.97 ± 0.48	6.03 ± 0.58	4.87 ± 0.11	<b>4.40 ± 0.10</b>	3.24 ± 0.10	3.06 ± 0.18	2.97 ± 0.02	<b>2.85 ± 0.02</b>
Energy	0.70 ± 0.38	2.09 ± 0.29	<b>0.35 ± 0.01</b>	0.41 ± 0.02	1.03 ± 0.35	1.38 ± 0.22	0.96 ± 0.13	<b>0.28 ± 0.11</b>
Kin8nm	–	0.09 ± 0.00	<b>0.07 ± 0.00</b>	0.19 ± 0.00	–	<b>-1.20 ± 0.02</b>	-1.09 ± 0.01	-0.20 ± 0.02
Naval	–	<b>0.00 ± 0.00</b>	<b>0.00 ± 0.00</b>	<b>0.00 ± 0.00</b>	–	-5.63 ± 0.05	<b>-7.17 ± 0.03</b>	-5.28 ± 0.02
Power	4.05 ± 0.12	4.11 ± 0.17	4.07 ± 0.04	<b>4.04 ± 0.05</b>	2.81 ± 0.03	2.79 ± 0.04	2.83 ± 0.01	<b>2.78 ± 0.01</b>
Protein	4.08 ± 0.06	4.71 ± 0.06	4.36 ± 0.02	<b>4.05 ± 0.03</b>	2.82 ± 0.01	2.83 ± 0.02	2.89 ± 0.01	<b>2.76 ± 0.00</b>
Wine	0.67 ± 0.03	0.64 ± 0.04	0.63 ± 0.01	<b>0.60 ± 0.02</b>	1.09 ± 0.10	0.94 ± 0.12	0.95 ± 0.01	<b>0.89 ± 0.02</b>
Yacht	1.46 ± 0.49	1.58 ± 0.48	<b>0.57 ± 0.05</b>	0.86 ± 0.07	1.79 ± 0.88	1.18 ± 0.21	<b>0.37 ± 0.08</b>	0.90 ± 0.09

Table 1: Results on UCI regression benchmark datasets comparing RMSE and NLL

### 3 Experiments and results

#### 3.1 Experimental setup and evaluation metrics

For a fair comparison with current state-of-the-art methods for predictive uncertainty estimation using NNs on benchmark regression tasks, we use the same experimental setup. The network consists of 50 hidden units with ReLU for smaller datasets split into 20 train-test folds and 100 units with ReLU for the larger ‘Protein’ dataset (5 folds). See Appendix C.1 for other training hyperparameters. We measure the NLL, a proper scoring rule and widely used metric for evaluating predictive uncertainty (Quinero-Candela et al. 2005). We also compute the root mean squared error (RMSE) to measure the performance of the single mean prediction of our model.

#### 3.2 Regression datasets: Toy regression and UCI regression benchmarks

To highlight the need for disentangled uncertainties, we first evaluate the performance of our method on an extension of the toy regression dataset setup and used to evaluate probabilistic backpropagation (PBP) (Hernández-Lobato and Adams 2015), deep ensembles (Lakshminarayanan, Pritzel, and Blundell 2017), and anchored ensembling (Pearce, Leibfried, and Brintrup 2020) which consists of 20 examples drawn from  $y = (x^3 + \epsilon)$  where  $\epsilon \sim \mathcal{N}(0, 3^2)$ . The extended multi-dimensional toy regression datasets, contain 40 examples each drawn from  $y = (x_1^3 + \epsilon_1)(x_2^3 + \epsilon_2)$  and  $y = (x_1^4 + \epsilon_1)(x_2^4 + \epsilon_2)$  where  $\epsilon_1, \epsilon_2 \sim \mathcal{N}(0, 3^2)$ . It can be observed that in the case of the unified uncertainty estimates, the underlying heteroscedasticity along each input feature can not be captured individually. However, using the same model architecture, our method can produce ‘different’ uncertainties for each input feature (Figure 1).

We then evaluate and compare our approach to current state-of-the-art methods for predictive uncertainty estimation using NNs on UCI regression benchmark datasets (see Appendix C.1 for details on datasets). Table 1 shows the comparison with the latest and competitive methods - RIO (Qiu,

Meyerson, and Miikkulainen 2020), deep ensembles (Lakshminarayanan, Pritzel, and Blundell 2017) and anchored ensembling (Pearce, Leibfried, and Brintrup 2020); see Appendix D.1 for a full comparison with other methods - VI (Graves 2011), PBP (Hernández-Lobato and Adams 2015), MC-dropout (Gal and Ghahramani 2016), deterministic VI (DVI) (Wu et al. 2018) and subspace inference (SI) (Izmailov et al. 2020). We observe that our method outperforms the existing methods on multiple datasets, while also disentangling the predictive uncertainties.

We also highlight the performance of our proposed MVN model trained with a unified loss, as compared to post-hoc ensembling (vanilla mixture of experts) of independent cluster-wise NN models. This serves as the baseline for a comparison of disentangled uncertainty estimates through the corresponding RMSE and cluster-wise NLL. For each dataset, we train deep ensemble per input cluster (DEPC) and anchored ensembling per input cluster (AEPC) following their respective training procedure. This results in a prediction and an uncertainty estimate per cluster. We then average the predictions across the clusters for the final prediction. Hence, we have an NLL per cluster and a single RMSE for the final prediction. Table 2 shows that deep split ensembles outperform DEPC and AEPC on NLL of every cluster as well as RMSE. We attribute this to the joint training of cluster-wise experts in deep split ensembles, as compared to the independent training of cluster-wise experts in DEPC and AEPC.

#### 3.3 Calibration and uncertainty evaluation

As a consequence of modelling disentangled predictive uncertainties during the training of NNs using NLL, we observe that our approach produces cluster-wise inherently well-calibrated models. Moreover, given that our model estimates disentangled uncertainties, we are able to assess the calibration of our model in a granular cluster-wise fashion. We assess our models without any post-hoc calibration. We first demonstrate this using entropy plots with out-of-distribution samples, and then using cluster-wise calibration curves using empirical rule.

**Entropy analyses with out-of-distribution samples:** In real-world settings, there are often dataset shifts where the

<sup>1</sup>NLLs of Deep Split Ensembles in Table 1 are averaged over feature clusters of corresponding datasets. Refer to Appendix D.3 for an exhaustive list of cluster-wise predictive uncertainty estimates for all datasets.

Datasets	RMSE			Clusters	Cluster-wise NLL		
	DEPC	AEPC	Deep Split Ens.		DEPC	AEPC	Deep Split Ens.
Boston	$5.11 \pm 1.06$	$4.93 \pm 1.03$	<b><math>2.53 \pm 0.15</math></b>	1	$2.91 \pm 0.16$	$3.87 \pm 0.82$	<b><math>2.23 \pm 0.04</math></b>
				2	$2.82 \pm 0.16$	$3.99 \pm 0.94$	<b><math>2.20 \pm 0.03</math></b>
				3	$3.29 \pm 0.10$	$4.23 \pm 1.06$	<b><math>2.26 \pm 0.05</math></b>
Concrete	$10.24 \pm 0.85$	$10.40 \pm 0.93$	<b><math>4.40 \pm 0.10</math></b>	1	$3.77 \pm 0.05$	$5.75 \pm 0.61$	<b><math>2.84 \pm 0.02</math></b>
				2	$3.79 \pm 0.09$	$5.68 \pm 0.60$	<b><math>2.85 \pm 0.02</math></b>
				3	$3.80 \pm 0.05$	$5.83 \pm 0.61$	<b><math>2.87 \pm 0.01</math></b>

Table 2: Results of deep ensemble per input cluster (DEPC), anchored ensembling per input cluster (AEPC), and deep split ensembles on UCI regression benchmark datasets<sup>2</sup> comparing RMSE and cluster-wise NLL.

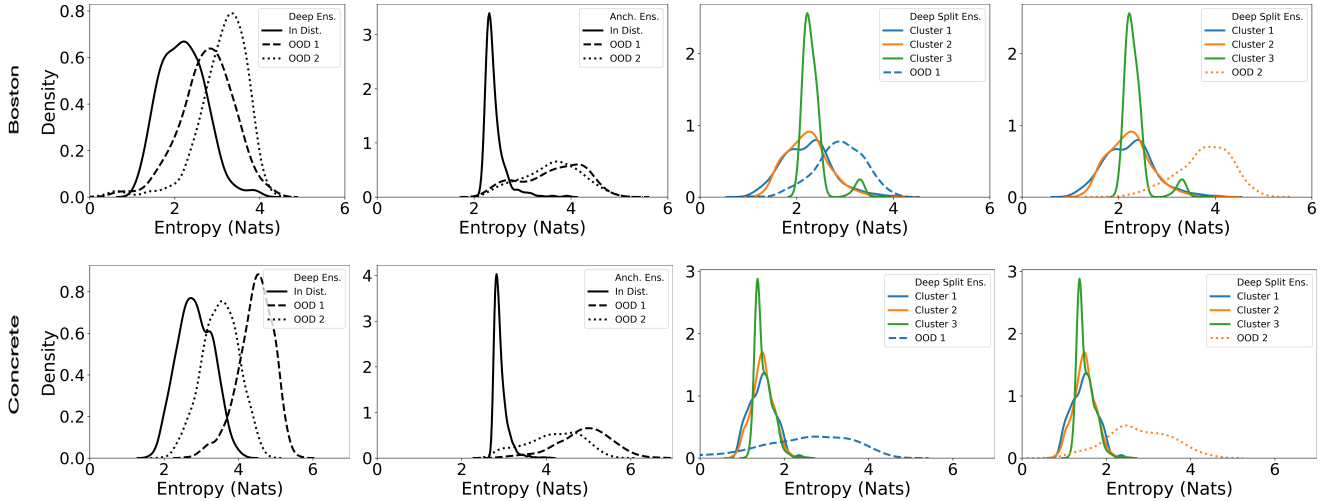


Figure 3: Entropy plots for ‘Boston’ and ‘Concrete’ datasets using hierarchical clustering (Section 2.3). The first two columns show the kernel density estimation (KDE) of entropy for in- distribution i.e.  $\mathcal{N}(0, 1)$  and out-of-distribution samples, obtained with unified uncertainty estimation using deep ensemble and anchored ensembling respectively. The last two columns show ‘cluster-wise’ KDE of entropy for in-distribution and out-of-distribution samples, obtained with disentangled uncertainty estimation using deep split ensembles. OOD 1 and OOD 2 refer to introducing dataset shift by inducing noise sampled from  $\mathcal{N}(6, 2^2)$  into 2 random input features; the features correspond to different clusters for deep split ensembles. See Appendix E.1 for similar analyses for all other datasets.

observed target data distribution may shift and eventually be very different once a model is deployed. Subsequently, the predictions need to exhibit higher uncertainty when this occurs. To assess it, we intentionally introduce a dataset shift by inducing noise, sampled from Gaussian distributions with shifted means and variances, into a random feature of a cluster and measure the corresponding clusters’ predicted entropy (Figure 3). We observe an increase in the entropy of only the noisy cluster while entropies of other clusters remain intact with deep split ensembles. However, unified uncertainty estimation methods like deep ensembles and anchored ensembling show an increase in the entropy corresponding to all features together. The disentanglement in OOD behaviour is an inherent characteristic of our method that cannot be observed in existing methods estimating unified uncertainties. Consequently, deep split ensembles can help better trace dataset shifts and pinpoint the noisy feature clusters during test time.

### ‘Cluster-wise’ calibration curves using empirical rule:

It is crucial to have good and stable calibration for reliable uncertainty estimates. To highlight our inherently well-calibrated models, we further evaluate to obtain calibration curves using the 68–95–99.7 rule (also called empirical rule). We first compute the  $x\%$  prediction interval for each test datapoint based on Gaussian quantiles using the predicted mean and variance. We then calculate the fraction of test observations (true values) that fall within this prediction interval. For a well-calibrated model, the observed fraction should be close to  $x\%$  calculated earlier. To see how our models perform in this setting, we sweep from  $x = 10\%$  to  $x = 90\%$  in steps of 10, and consequently a line lying very close to the line  $y = x$  would indicate a well-calibrated model. Here, we further define stability of ‘cluster-wise’ calibration as having similar calibration curves across clusters. As this experiment aims to test the calibration of the model with respect to each

<sup>2</sup>Refer to Appendix D.3 for results on all other datasets.

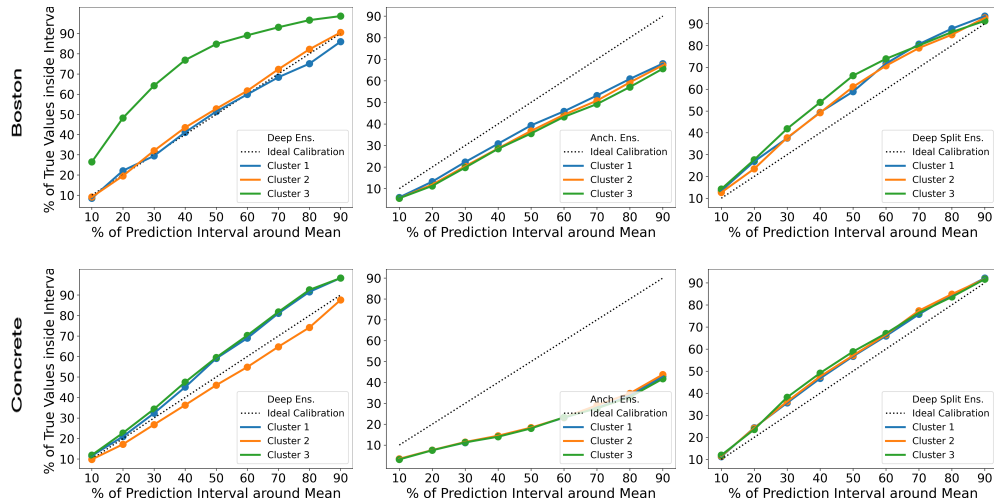


Figure 4: ‘Cluster-wise’ calibration curves using empirical rule for ‘Boston’ and ‘Concrete’ datasets using hierarchical clustering (Section 2.3). The columns contain experiments using deep ensemble per input cluster (DEPC), anchored ensembling per input cluster (AEPC) and deep split ensembles respectively. See Appendix E.2 for similar analyses on all other datasets

Datasets	RMSE			Clusters ( $C$ )	Cluster-wise NLL		
	DEPC	AEPC	Deep Split Ens.		DEPC	AEPC	Deep Split Ens.
Power	$4.90 \pm 0.23$	$4.91 \pm 0.22$	<b><math>4.07 \pm 0.04</math></b>	$C_{p1}$	$2.99 \pm 0.04$	$3.08 \pm 0.07$	<b><math>2.81 \pm 0.05</math></b>
				$C_{p2}$	$3.13 \pm 0.03$	$3.08 \pm 0.07$	<b><math>2.83 \pm 0.05</math></b>
Wine	$0.64 \pm 0.04$	$0.66 \pm 0.05$	<b><math>0.59 \pm 0.02</math></b>	$C_{w1}$	$0.94 \pm 0.06$	$1.02 \pm 0.09$	<b><math>0.88 \pm 0.02</math></b>
				$C_{w3}$	$0.96 \pm 0.06$	$1.03 \pm 0.09$	<b><math>0.89 \pm 0.03</math></b>
				$C_{w3}$	$0.94 \pm 0.07$	$1.03 \pm 0.09$	<b><math>0.90 \pm 0.04</math></b>

Table 3: Results with clusters from human experts for the two datasets below. See Appendix A.2 for list of clusters ( $C$ ).

of the clusters individually, we use DEPC and AEPC to produce more suitable baselines to compare our method more rigorously. Figure 4 shows the calibration curves for each feature cluster for the different methods. We notice that deep split ensembles have a more uniform and stable calibration across clusters.

### 3.4 Deep split ensembles based on domain knowledge and/or user needs

We illustrate how deep split ensembles allow for modelling predictive uncertainties using domain knowledge and/or user needs by taking in such clusters of input feature space. This is important as it brings the human in the loop and helps better define the task qualitatively. We consulted human experts, for the ‘Power’ and ‘Wine’ datasets, to qualitatively cluster the input features based on the uncertainties they would desire from a machine learning system trained on those datasets (details in Appendix A.2). We then trained a deep split ensemble, DEPC and AEPC using the same experimental setup as above. Table 3 shows that the results of deep split ensembles here are comparable to results in Table 1, while outperforming DEPC and AEPC. The consistent improved performance upon changing the constituents of the clusters of input features demonstrates the inherent flexibility available while

training deep split ensembles.

### 3.5 Deep split ensembles in multi-modal settings

The split nature of deep split ensembles makes them suitably applicable in multi-modal settings as heteroscedasticity in data can be highly decoupled due to the individual nature of the modalities. Each cluster of input features can be used to represent a particular modality of the input feature space to obtain a predictive uncertainty per modality.

To demonstrate this in a safety-critical application, we use a multi-modal Alzheimer’s dementia (AD) dataset, ‘ADReSS’, consisting of speech samples (audio) and their transcriptions (text), to regress MMSE<sup>3</sup> scores. The standardized dataset contains 108 train and 48 heldout-test subjects. The train set is further split into 80%-20% train-validation sets. We first devise a feature engineering pipeline that extracts several multi-modal cognitive and acoustic feature sets - interventions, disfluency, and acoustic - based on domain knowledge and context. We then train a deep split NN with those feature sets. The deep splits corresponding to disfluency

<sup>3</sup>Mini-Mental State Examination (MMSE) scores, ranging from 0 to 30, offers a way to quantify cognitive function and screen for cognitive loss by testing the individuals’ attention, recall, language and motor skills (Tombaugh and McIntyre 1992).

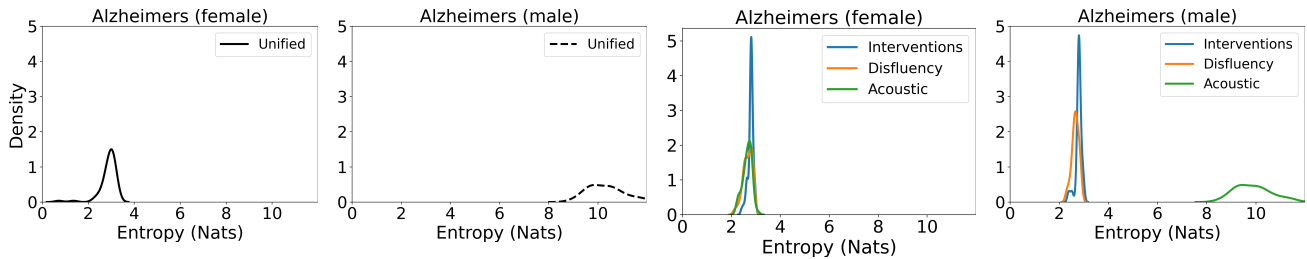


Figure 5: Entropy plots for Alzheimer’s dataset showing the kernel density estimation (KDE) for male and female subjects specifically. The first two plots indicate unified uncertainty estimation using deep ensembles while the last two plots show disentangled uncertainty estimation using deep split ensembles. Both the methods are trained on female subjects and evaluated on male subjects to highlight hidden ‘modality-specific’ gender bias.

and acoustic feature sets are fully connected and that corresponding to interventions feature set is an LSTM. See Appendix C.2 for details about the dataset, feature sets, model architecture and hyperparameters. Our method shows improved performance over state-of-the-art RMSE results, while also estimating a predictive uncertainty for each modality (Table 4). We attribute this observation to the variance-affected learning rate (Nix and Weigend 1994) which would help stabilize multi-modal training. We further train a deep ensemble for comparison on predictive uncertainty estimates, and observe that deep split ensemble achieves a better RMSE as well as a better NLL in each of the modalities.

To assess the calibration of our model and highlight potential hidden bias in real-world settings, we then train on only female subjects and evaluate it on only male subjects from the dataset. This would induce a bias in the model, which can be illustrated with the predicted uncertainties, as two modes (disfluency and interventions) are gender neutral by nature, whereas acoustic features can significantly vary. Consequently, upon experimentation (Figure 5), we observe that the entropy corresponding to all modalities together increases on the male inputs in case of unified uncertainty estimation using deep ensemble. However, in case of disentangled uncertainty estimation using deep split ensemble, only the entropy of the acoustic feature set on the male inputs significantly increases. The high predicted uncertainty corresponding to acoustic features for only male subjects highlights the hidden ‘modality-specific’ gender bias.

Model	RMSE	NLL
Pappagari et al. (2020)	5.37	–
Luz et al. (2020)	5.20	–
Sarawgi et al. (2020)	4.60	–
Balagopalan et al. (2020)	4.56	–
Rohanian, Hough, and Purver	4.54	–
Deep Ensemble	4.90	3.08
<b>Deep Split Ensemble</b>	<b>4.37</b>	<b>2.94, 2.98, 2.94</b>

Table 4: Test results on multi-modal ADReSS dataset for MMSE score regression.

## 4 Discussion and future work

We have proposed a conceptually simple yet effective non-Bayesian method, *deep split ensembles*, to estimate disentangled predictive uncertainties using NNs for input feature clusters. Disentangling a unified uncertainty allows for granular information about plausible sources of heteroscedasticity in the data. This is important in safety-critical settings as it enables improved risk assessment and decision-making. One can further form clusters containing one feature each to estimate feature-wise uncertainties. Using thus produced entropy values, noisy features or clusters can be suppressed while training a more reliable model for the same dataset with potentially improved performance. This encourages interoperability between humans and models in a unique way. Our method also reduces computational costs through sparser clusterwise connections, requires few changes in the NN, and can be readily implemented and trained. The nature of the split NN structure facilitates intuitive model-parallelism training for large models in multi-GPU systems where each cluster can be placed in separate GPUs. Using domain knowledge from human experts, deep split ensembles can help satisfy user needs by generating different combinations of uncertainty estimates desired from a machine learning system, thus providing a more controllable form of reliability and awareness with the model. The potential to highlight hidden biases, such as shown in multi-modal settings, has immediate and apparent real world applications to mitigate unseen biases in deployed models. This serves as a motivation for fair and aware systems supporting human-assisted AI.

A direct extension of our work would be to use complex distributions such as mixture density networks (Bishop 1994) for modelling output distributions. There are many exciting future directions, such as unsupervised learning to form deeper representation for the clusters of features (Xie, Girschick, and Farhadi 2016), using uncertainty attention (Heo et al. 2018; Lee et al. 2018) to aid in training of the ensemble classifiers, exploring adaptive defer systems (Madras, Pitassi, and Zemel 2018) along with partial deferring based on clusters for better calibration of uncertainties coupled with human experts, and considering uncertainty of human feedback (He, Chen, and An 2020).

## References

- Amodei, D.; Olah, C.; Steinhardt, J.; Christiano, P.; Schulman, J.; and Mané, D. 2016. Concrete problems in AI safety. *arXiv preprint arXiv:1606.06565* .
- Ashukha, A.; Lyzhov, A.; Molchanov, D.; and Vetrov, D. 2020. Pitfalls of in-domain uncertainty estimation and ensembling in deep learning. *arXiv preprint arXiv:2002.06470* .
- Balagopalan, A.; Eyre, B.; Rudzicz, F.; and Novikova, J. 2020. To BERT or Not To BERT: Comparing Speech and Language-based Approaches for Alzheimer’s Disease Detection. *arXiv preprint arXiv:2008.01551* .
- Bishop, C. M. 1994. Mixture density networks .
- Blundell, C.; Cornebise, J.; Kavukcuoglu, K.; and Wierstra, D. 2015. Weight Uncertainty in Neural Network. In Bach, F.; and Blei, D., eds., *Proceedings of the 32nd International Conference on Machine Learning*, volume 37 of *Proceedings of Machine Learning Research*, 1613–1622. Lille, France: PMLR. URL <http://proceedings.mlr.press/v37/blundell15.html>.
- Dietterich, T. G. 2000. Ensemble methods in machine learning. In *International workshop on multiple classifier systems*, 1–15. Springer.
- Dusenberry, M. W.; Tran, D.; Choi, E.; Kemp, J.; Nixon, J.; Jerfel, G.; Heller, K.; and Dai, A. M. 2020. Analyzing the role of model uncertainty for electronic health records. In *Proceedings of the ACM Conference on Health, Inference, and Learning*, 204–213.
- Dutt, A.; Pellerin, D.; and Quénot, G. 2020. Coupled ensembles of neural networks. *Neurocomputing* 396: 346–357.
- Furlanello, T.; Lipton, Z. C.; Tschannen, M.; Itti, L.; and Anandkumar, A. 2018. Born again neural networks. *arXiv preprint arXiv:1805.04770* .
- Gal, Y. 2016. Uncertainty in deep learning. *University of Cambridge* 1: 3.
- Gal, Y.; and Ghahramani, Z. 2016. Dropout as a bayesian approximation: Representing model uncertainty in deep learning. In *international conference on machine learning*, 1050–1059.
- Graves, A. 2011. Practical Variational Inference for Neural Networks. In Shawe-Taylor, J.; Zemel, R. S.; Bartlett, P. L.; Pereira, F.; and Weinberger, K. Q., eds., *Advances in Neural Information Processing Systems 24*, 2348–2356. Curran Associates, Inc. URL <http://papers.nips.cc/paper/4329-practical-variational-inference-for-neural-networks.pdf>.
- Guo, C.; Pleiss, G.; Sun, Y.; and Weinberger, K. Q. 2017. On calibration of modern neural networks. In *Proceedings of the 34th International Conference on Machine Learning-Volume 70*, 1321–1330. JMLR. org.
- He, X.; Chen, H.; and An, B. 2020. Learning Behaviors with Uncertain Human Feedback. *arXiv preprint arXiv:2006.04201* .
- Heo, J.; Lee, H. B.; Kim, S.; Lee, J.; Kim, K. J.; Yang, E.; and Hwang, S. J. 2018. Uncertainty-aware attention for reliable interpretation and prediction. In *Advances in Neural Information Processing Systems*, 909–918.
- Hernández-Lobato, J. M.; and Adams, R. 2015. Probabilistic backpropagation for scalable learning of bayesian neural networks. In *International Conference on Machine Learning*, 1861–1869.
- Hinton, G. 1999. Product of experts. In *Proceedings of the International Conference on Artificial Neural Networks vol. 1*, 1–6.
- Izmailov, P.; Maddox, W. J.; Kirichenko, P.; Garipov, T.; Vetrov, D.; and Wilson, A. G. 2020. Subspace inference for Bayesian deep learning. In *Uncertainty in Artificial Intelligence*, 1169–1179. PMLR.
- Jacobs, R. A.; Jordan, M. I.; Nowlan, S. J.; and Hinton, G. E. 1991. Adaptive mixtures of local experts. *Neural computation* 3(1): 79–87.
- Jain, S.; Liu, G.; Mueller, J.; and Gifford, D. 2020. Maximizing Overall Diversity for Improved Uncertainty Estimates in Deep Ensembles. In *AAAI*, 4264–4271.
- Kay, J. W.; Titterton, D. M.; et al. 1999. *Statistics and neural networks: advances at the interface*. Oxford University Press on Demand.
- Kendall, A.; and Gal, Y. 2017. What uncertainties do we need in bayesian deep learning for computer vision? In *Advances in neural information processing systems*, 5574–5584.
- Kingma, D.; Salimans, T.; and Welling, M. 2015. Variational Dropout and the Local Reparameterization Trick .
- Kuleshov, V.; Fenner, N.; and Ermon, S. 2018. Accurate uncertainties for deep learning using calibrated regression. *arXiv preprint arXiv:1807.00263* .
- Kumar, A.; Liang, P. S.; and Ma, T. 2019. Verified uncertainty calibration. In *Advances in Neural Information Processing Systems*, 3787–3798.
- Lakshminarayanan, B.; Pritzel, A.; and Blundell, C. 2017. Simple and scalable predictive uncertainty estimation using deep ensembles. In *Advances in neural information processing systems*, 6402–6413.
- LeCun, Y.; Bengio, Y.; and Hinton, G. 2015. Deep learning. *nature* 521(7553): 436–444.
- Lee, H. B.; Lee, J.; Kim, S.; Yang, E.; and Hwang, S. J. 2018. DropMax: adaptive variational softmax. In *Advances in Neural Information Processing Systems*, 919–929.
- Lee, J.; Bahri, Y.; Novak, R.; Schoenholz, S. S.; Pennington, J.; and Sohl-Dickstein, J. 2017. Deep neural networks as gaussian processes. *arXiv preprint arXiv:1711.00165* .
- Lee, S.; Purushwalkam, S.; Cogswell, M.; Crandall, D.; and Batra, D. 2015. Why M heads are better than one: Training a diverse ensemble of deep networks. *arXiv preprint arXiv:1511.06314* .
- Luz, S.; Haider, F.; de la Fuente, S.; Fromm, D.; and MacWhinney, B. 2020. Alzheimer’s Dementia Recognition through Spontaneous Speech: The ADReSS Challenge. *arXiv preprint arXiv:2004.06833* .



- MacKay, D. J. C. 1992. A Practical Bayesian Framework for Backpropagation Networks. *Neural Comput.* 4(3): 448–472. ISSN 0899-7667. doi:10.1162/neco.1992.4.3.448. URL <https://doi.org/10.1162/neco.1992.4.3.448>.
- Madras, D.; Pitassi, T.; and Zemel, R. 2018. Predict responsibly: improving fairness and accuracy by learning to defer. In *Advances in Neural Information Processing Systems*, 6147–6157.
- Nix, D. A.; and Weigend, A. S. 1994. Estimating the mean and variance of the target probability distribution. In *Proceedings of 1994 IEEE International Conference on Neural Networks (ICNN'94)*, volume 1, 55–60. IEEE.
- Osband, I. 2016. Risk versus Uncertainty in Deep Learning : Bayes , Bootstrap and the Dangers of Dropout.
- Pappagari, R.; Cho, J.; Moro-Velazquez, L.; and Dehak, N. 2020. Using state of the art speaker recognition and natural language processing technologies to detect Alzheimer’s disease and assess its severity .
- Pearce, T.; Leibfried, F.; and Brintrup, A. 2020. Uncertainty in neural networks: Approximately Bayesian ensembling. In *International conference on artificial intelligence and statistics*, 234–244. PMLR.
- Platt, J. C. 1999. Probabilistic Outputs for Support Vector Machines and Comparisons to Regularized Likelihood Methods. In *ADVANCES IN LARGE MARGIN CLASSIFIERS*, 61–74. MIT Press.
- Qiu, X.; Meyerson, E.; and Miikkulainen, R. 2020. Quantifying Point-Prediction Uncertainty in Neural Networks via Residual Estimation with an I/O Kernel. In *International Conference on Learning Representations*. URL <https://openreview.net/forum?id=rkxNh1Stvr>.
- Quinonero-Candela, J.; Rasmussen, C. E.; Sinz, F.; Bousquet, O.; and Schölkopf, B. 2005. Evaluating predictive uncertainty challenge. In *Machine Learning Challenges Workshop*, 1–27. Springer.
- Rohanian, M.; Hough, J.; and Purver, M. 2020. Multi-modal Fusion with Gating using Audio, Lexical and Disfluency Features for Alzheimer’s Dementia Recognition from Spontaneous Speech .
- Sarawgi, U.; Zulfikar, W.; Soliman, N.; and Maes, P. 2020. Multimodal Inductive Transfer Learning for Detection of Alzheimer’s Dementia and its Severity. *arXiv preprint arXiv:2009.00700* .
- Shridhar, K.; Laumann, F.; and Liwicki, M. 2018. Uncertainty estimations by softplus normalization in bayesian convolutional neural networks with variational inference. *arXiv preprint arXiv:1806.05978* .
- Snoek, J.; Ovadia, Y.; Fertig, E.; Lakshminarayanan, B.; Nowozin, S.; Sculley, D.; Dillon, J.; Ren, J.; and Nado, Z. 2019. Can you trust your model’s uncertainty? Evaluating predictive uncertainty under dataset shift. In *Advances in Neural Information Processing Systems*, 13969–13980.
- Thiagarajan, J. J.; Venkatesh, B.; Sattigeri, P.; and Bremer, P.-T. 2020. Building Calibrated Deep Models via Uncertainty Matching with Auxiliary Interval Predictors. In *AAAI*, 6005–6012.
- Tombaugh, T. N.; and McIntyre, N. J. 1992. The mini-mental state examination: a comprehensive review. *Journal of the American Geriatrics Society* 40(9): 922–935.
- Varshney, K. R.; and Alemzadeh, H. 2017. On the safety of machine learning: Cyber-physical systems, decision sciences, and data products. *Big data* 5(3): 246–255.
- Welling, M.; and Teh, Y. W. 2011. Bayesian Learning via Stochastic Gradient Langevin Dynamics. In *Proceedings of the 28th International Conference on International Conference on Machine Learning, ICML’11*, 681–688. Madison, WI, USA: Omnipress. ISBN 9781450306195.
- Williams, C.; Agakov, F. V.; and Felderhof, S. N. 2002. Products of gaussians. In *Advances in neural information processing systems*, 1017–1024.
- Wu, A.; Nowozin, S.; Meeds, E.; Turner, R. E.; Hernández-Lobato, J. M.; and Gaunt, A. L. 2018. Deterministic variational inference for robust bayesian neural networks. *arXiv preprint arXiv:1810.03958* .
- Xie, J.; Girshick, R.; and Farhadi, A. 2016. Unsupervised deep embedding for clustering analysis. In *International conference on machine learning*, 478–487.
- Xu, L.; Jordan, M. I.; and Hinton, G. E. 1995. An alternative model for mixtures of experts. In *Advances in neural information processing systems*, 633–640.

### Broader and ethical impact

Uncertainty estimations are crucial when employing black box neural networks (NNs) in sensitive and critical applications such as healthcare and self-driving cars. These NNs often tend to be over confident of their predictions; the confidence measures are not a true estimate of the model’s performance. Predicting the uncertainties can help in better understanding how confident the model is in its predictions and reflect upon the noise introduced by the stochastic data generation processes. It is important to know what the model is unsure about. Although current NNs can demonstrate high performance on test datasets, they sometimes tend to fail when deployed in real world settings due to noisy real-world data and dataset shifts.

A unified uncertainty estimation helps in providing confidence estimates. Further disentangling the unified predictive uncertainties give deeper insights into the various feature clusters and their associated heteroscedasticity. We believe that anyone who is involved in synergy with a machine learning system in decision making will benefit from such systems. For example, when such a system is deployed in a hospital setting to stratify the risk of a disease/condition, the doctor can understand the uncertainties associated with each input feature modality, and is able to better interpret the model’s belief. In such high-risk and safety-critical settings, deploying a black box NN could be sub-optimal. Additionally, multidisciplinary machine learning researchers will benefit from this as they will have a tool to better incorporate domain knowledge and user demands/needs.

# Appendix

## A Feature Clusters

### A.1 Feature clusters from hierarchical clustering

As discussed in Section 2.3, the input feature space is split into  $k$  exhaustive clusters using hierarchical clustering based on Pearson correlation distance. The dendrograms thus obtained upon hierarchical clustering with complete linkage are thresholded relative to the maximum distance to obtain feature clusters (Figure 6); we chose 0.5 and 0.75 to span a variety of number of clusters and features per cluster. One can change this threshold value to obtain different sets of feature clusters. Table 5 enlists the clusters thus obtained for each dataset.

### A.2 Feature clusters from human experts

As discussed in Section 3.4, we consulted human experts, for the ‘Power Plant Output’ and ‘Red Wine Quality’ datasets, to qualitatively cluster the input features based on the uncertainties desired from a machine learning system trained on those datasets. Table 6 shows the features cluster thus obtained, and the reasons as mentioned by the human experts are summarized below:

- ‘Power Plant Output’: While the Vacuum is collected from and has effect on the Steam Turbine, the three other ambient variables effect the GT performance.
- ‘Red Wine Quality’: Alcohol, pH, fixed acidity, density, and residual sugar are resultant characteristics of the wine. Volatile acidity and citric acid are added acidity in the wine-making. Chlorides, free sulphur dioxide, total sulphur dioxide, and sulphates are preservatives and antibacterials.

## B Derivations and proofs

### B.1 Derivations of $\mu$ and $\sigma$ of a Gaussian mixture

Given a Gaussian mixture  $p_E(\mathbf{y}|\mathbf{x})$ , where  $p_E(\mathbf{y}|\mathbf{x}) = E^{-1} \sum_e \mathcal{N}(\mu_{\theta_e}(\mathbf{x}), \Sigma_{\theta_e}(\mathbf{x}))$ , let the mean and the variance of the mixture be  $\mu_E(\mathbf{x})$  and  $\Sigma_E(\mathbf{x})$  respectively. Let  $t \sim E^{-1} \sum_e \mathcal{N}(\mu_{\theta_e}(\mathbf{x}), \Sigma_{\theta_e}(\mathbf{x}))$ .

#### Derivation of the mean of a Gaussian mixture

$t = z + \epsilon$ , where  $z = \mu_{\theta_e}(\mathbf{x})$  with equal probability  $E^{-1}$  for  $e = 1, 2, \dots, E$  and the conditional probability distribution of  $\epsilon$  given  $z$  will be  $N(0, \Sigma_{\theta_e}(\mathbf{x}))$ .

$$\mu_E(\mathbf{x}) = E[t]$$

$$\implies \mu_E(\mathbf{x}) = E[E[t|z]]$$

$$\implies \mu_E(\mathbf{x}) = E \left\{ \begin{array}{l} \vdots \\ \mu_{\theta_e}(\mathbf{x}) \quad \text{with probability } E^{-1} \\ \vdots \end{array} \right\}$$

$$\implies \mu_E(\mathbf{x}) = E^{-1} \sum_{e=1}^E \mu_{\theta_e}(\mathbf{x}) \quad (8)$$

### Derivation of the variance of a Gaussian mixture

We have,

$$\text{var}(t) = E[\text{var}(t|z)] + \text{var}(E[t|z])$$

$$\implies \text{var}(t) = E \left\{ \begin{array}{l} \vdots \\ \Sigma_{\theta_e}(\mathbf{x}) \quad \text{with probability } E^{-1} \\ \vdots \end{array} \right\} + \text{var} \left\{ \begin{array}{l} \vdots \\ \mu_{\theta_e}(\mathbf{x}) \quad \text{with probability } E^{-1} \\ \vdots \end{array} \right\}$$

$$\implies \text{var}(t) = E^{-1} \sum_{e=1}^E \Sigma_{\theta_e}(\mathbf{x}) + E^{-1} \sum_{e=1}^E (\mu_{\theta_e}(\mathbf{x}) - \mu_E(\mathbf{x}))(\mu_{\theta_e}(\mathbf{x}) - \mu_E(\mathbf{x}))^T$$

Using Equation (8) and given our assumption that the outputs of deep splits (in a deep split NN) are linearly uncorrelated, we have,

$$\Sigma_E(\mathbf{x}) = \text{diag}(\sigma_E^2(\mathbf{c}^1), \dots, \sigma_E^2(\mathbf{c}^k))$$

$$\sigma_E^2(\mathbf{c}^i) = E^{-1} \sum_{e=1}^E (\sigma_{\theta_e}^2(\mathbf{c}^i) + \mu_{\theta_e}^2(\mathbf{c}^i)) - \mu_E^2(\mathbf{c}^i)$$

## C Details of datasets, model and hyperparameters

### C.1 Benchmark regression datasets

Table 7 shows some statistics of the 9 benchmark regression datasets used in our experiments (Section 3). We have included all the datasets in the Supplementary Material provided. The hyperparameters used for training the deep split ensembles are enlisted in Table 8. For anchored ensembling per feature cluster (AEPC) and deep ensembles per feature cluster (DEPC), we use the hyperparameters mentioned in the anchored ensembling and deep ensembles papers respectively.

### C.2 Alzheimer’s dementia (AD) - dataset, model and hyperparameters

#### Dataset

The ADReSS (Alzheimer’s Dementia Recognition through Spontaneous Speech) dataset, available through the benchmark DementiaBank database upon access request, is a standardized and balanced dataset of 156 speech samples, each from a unique subject, matched for age and gender. The dataset consists of speech recordings and transcripts of spoken picture descriptions elicited from participants through

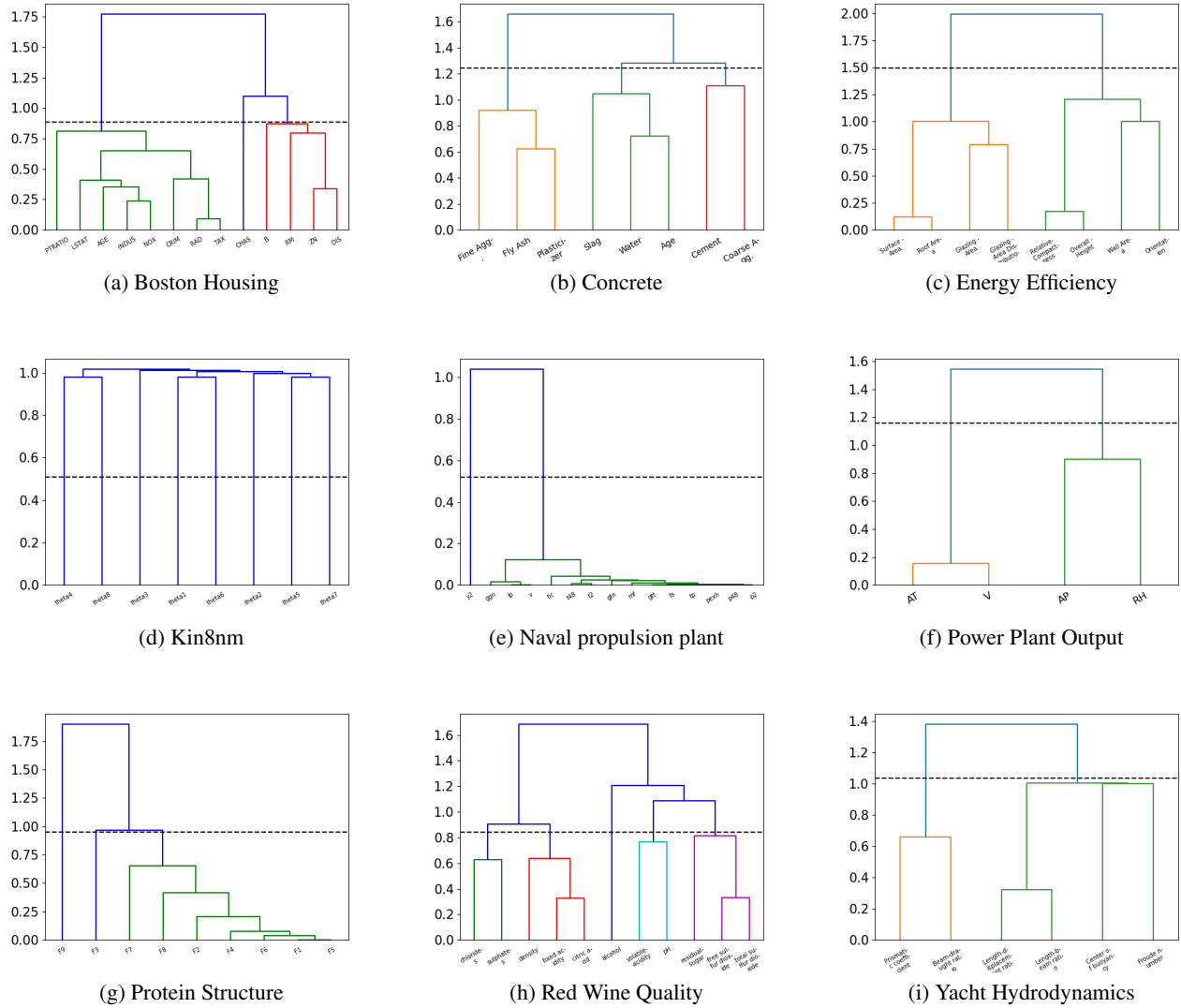


Figure 6: Dendrograms obtained for UCI datasets upon hierarchical clustering of features based on Pearson correlation distance. The dotted line shows the threshold value used to extract clusters.

the Cookie Theft picture from the Boston Diagnostic Aphasia Exam. The dataset also provides corresponding Mini-Mental Status Examination (MMSE) scores, ranging from 0 to 30, of the subjects, which offers a way to quantify cognitive function and screen for cognitive loss by testing the individuals' orientation, attention, calculation, recall, language and motor skills. These scores are used as labels for the regression task. A standardized train-test split of around 70%-30% (108 and 48 subjects) is provided by this dataset. The test set is held-out until final evaluation, and the train set is split into train and validation sets for training models. This dataset was used for evaluating deep split ensembles in multi-modal settings (Section 3.5).

### Multi-modal feature engineering pipeline

People with dementia show symptoms of cognitive decline, impairment in memory, communication and thinking. To include such domain knowledge and context, we devised an automated feature engineering pipeline that extracts several multi-modal cognitive and acoustic feature sets - interventions, disfluency, and acoustic. These three feature sets are then fed to a deep split NN, model architecture of which is shown in Figure 7. Similar extracted features have been repeatedly used to propose speech recognition based solutions for automated detection of mild cognitive impairment from spontaneous speech. The three extracted feature sets are as follows:

- *Interventions features*: Cognitive features reflect upon potential loss of train of thoughts and context. Our system extracts the sequence of speakers from the transcripts, cat-

Dataset	Cluster	Features
Boston Housing	1	CRIM, INDUS, NOX, AGE, RAD, TAX, PTRATIO, LSTAT
	2	ZN, RM, DIS, B
	3	CHAS
Concrete	1	Fly Ash, Superplasticizer, Fine Aggregate
	2	Water, Age, Blast Furnace Slag
	3	Cement, Coarse Aggregate
Energy Efficiency	1	Surface Area, Roof Area, Glazing Area, Glazing Area Distribution
	2	Relative Compactness, Overall Height, Wall Area, Orientation
Kin8nm	1	theta1
	2	theta2
	3	theta3
	4	theta4
	5	theta5
	6	theta6
	7	theta7
	8	theta8
Naval Propulsion Plant	1	lp, v, ggn
	2	ggt, gtn, ts, tp, t48, t2, p48, p2, pexh, tic, mf
Power Plant Output	1	AT, V
	2	AP, RH
Protein Structure	1	F1, F2, F4, F5, F6, F7, F8
	2	F3
	3	F9
Red Wine Quality	1	chlorides, sulphates
	2	fixed acidity, citric acid, density
	3	volatile acidity, pH
	4	residual sugar, free sulfur dioxide, total sulfur dioxide
	5	alcohol
Yacht Hydrodynamics	1	Prismatic coefficient, Beam-draught ratio
	2	Length-displacement ratio, Length-beam ratio, Longitudinal position, Froude number

Table 5: List of feature clusters obtained for UCI datasets using hierarchical clustering.

Dataset	Cluster	Features
Power Plant Output	$C_{p1}$	AT, AP, RH
	$C_{p2}$	V
Red Wine Quality	$C_{w1}$	alcohol, pH, fixed acidity, density, residual sugar
	$C_{w2}$	volatile acidity, citric acid
	$C_{w3}$	chlorides, free sulphur dioxide, total sulphur dioxide, sulphates

Table 6: List of feature clusters obtained for ‘Power’ and ‘Wine’ UCI datasets from human experts.

egorizing it as the subject or the interviewer. To accommodate for the variable length of these sequences, they are padded or truncated to length of 32 steps, found upon analyses and tuning of sequence lengths. These (subject, interviewer, or padding) are then one-hot encoded resulting in 32x3 input size for this feature set corresponding to every datapoint.

- *Disfluency features*: A set of 11 distinct and carefully curated features from the transcripts; word rate, intervention

rate, and 9 different kinds of pause rates, reflecting upon speech impediments like slurring and stuttering. These are normalized by the respective audio lengths and scaled thereafter.

- *Acoustic features*: The ComParE 2013 feature set<sup>4</sup> was extracted from the audio samples using the open-sourced

<sup>4</sup><https://dl.acm.org/doi/abs/10.1145/2502081.2502224>,  
<https://dl.acm.org/doi/abs/10.1145/2502081.2502224>

Dataset	No. of datapoints	No. of features
Boston Housing	506	13
Concrete	1,030	8
Energy Efficiency	768	8
Kin8nm	8,192	8
Naval propulsion plant	11,934	16
Power Plant Output	9,568	4
Protein Structure	45,730	9
Red Wine Quality	1,599	11
Yacht Hydrodynamics	308	6

Table 7: UCI Benchmark regression dataset details

Dataset	Learning Rate	Epochs	Batch Size
Boston Housing	0.1	1000	100
Concrete	0.01	1500	32
Energy Efficiency	0.01	1500	16
Kin8nm	0.1	1000	100
Naval Propulsion Plant	0.01	1500	32
Power Plant Output	0.01	2500	256
Protein Structure	0.01	4000	1024
Red Wine Quality	0.1	1000	100
Yacht Hydrodynamics	0.01	1500	8

Table 8: Hyperparameters used to train deep split ensembles

openSMILE v2.1 toolkit, widely used for affect analyses in speech. This provides a total of 6,373 features that include energy, MFCC, and voicing related low-level descriptors (LLDs), and other statistical functionals. This feature set encodes changes in speech of a person and has been used as an important noninvasive marker for AD detection. Our system standardizes this set of features using z-score normalization, and uses principal component analysis (PCA) to project the 6,373 features onto a low-dimensional space of 21 orthogonal features with highest variance. The number of orthogonal features was selected by analyzing the percentage of variance explained by each of the components.

## Model architecture

The three feature sets are then fed to a deep split NN, the model architecture of which is shown in Figure 7.

## Setup and hyperparameters

Table 9 shows the setup and hyperparameters for the ADReSS dataset. Best model was saved upon monitoring negative log-likelihood of the validation set (val NLL).

Train-val split	80%-20% (86-22 datapoints)
Heldout-test set	48 datapoints
Optimizer	Adam
Learning rate	0.001
Batch size	8

Table 9: Setup and hyperparameters for the ADReSS dataset

## D Results on benchmark regression datasets

### D.1 Comparison with state-of-the-art methods

Tables 10 and 11 compare the RMSE and NLL<sup>5</sup> of our method on benchmark regression datasets with other state-of-the-art methods - particularly VI (Graves 2011), PBP (Hernández-Lobato and Adams 2015), MC-dropout (Gal and Ghahramani 2016), deterministic VI (DVI) (Wu et al. 2018) and subspace inference (SI) (Izmailov et al. 2020).

### D.2 Results of variants of deep split ensembles

Table 12 shows the RMSE and NLL<sup>5</sup> results of variants of deep split ensemble, with different number of models  $E = 1, 5, 10$  in the parallel ensemble. We observe that  $E = 5$  is the best of all considering the performance results and the computational overhead.

### D.3 Cluster-wise NLLs

Table 13 shows an exhaustive list of NLLs of all clusters for different number of models  $E$  in the parallel ensemble. Table 12 shows the average of these cluster-wise NLLs corresponding to each dataset. Table 14 shows NLL per cluster for DSE, AEPC, DEPC.

## E Experiments

### E.1 Entropy analyses

Figures 8 and 9 show the entropy plots for several datasets using hierarchical clustering and clusters from human experts. The first two columns show the kernel density estimation (KDE) of entropy for in- distribution i.e.  $\mathcal{N}(0, 1)$  and out-of-distribution samples, obtained with unified uncertainty estimation using deep ensemble and anchored ensembling respectively. The last two columns show ‘cluster-wise’ KDE of entropy for in-distribution and out-of-distribution samples, obtained with disentangled uncertainty estimation using deep split ensembles. OOD 1 and OOD 2 refer to introducing dataset shift by inducing noise sampled from  $\mathcal{N}(6, 2^2)$  into 2 random input features; the features correspond to different clusters for deep split ensembles. We used the entire datasets by accumulating fold-wise test results. The shift in the KDE (for OOD samples) of the cluster-wise entropy shows that the deep split ensembles are well-calibrated.

<sup>5</sup>NLLs of Deep Split Ensembles in Tables 11 and 12 are averaged over feature clusters of corresponding datasets. See Appendix D.3 for an exhaustive list of cluster-wise predictive uncertainty estimates for all datasets.

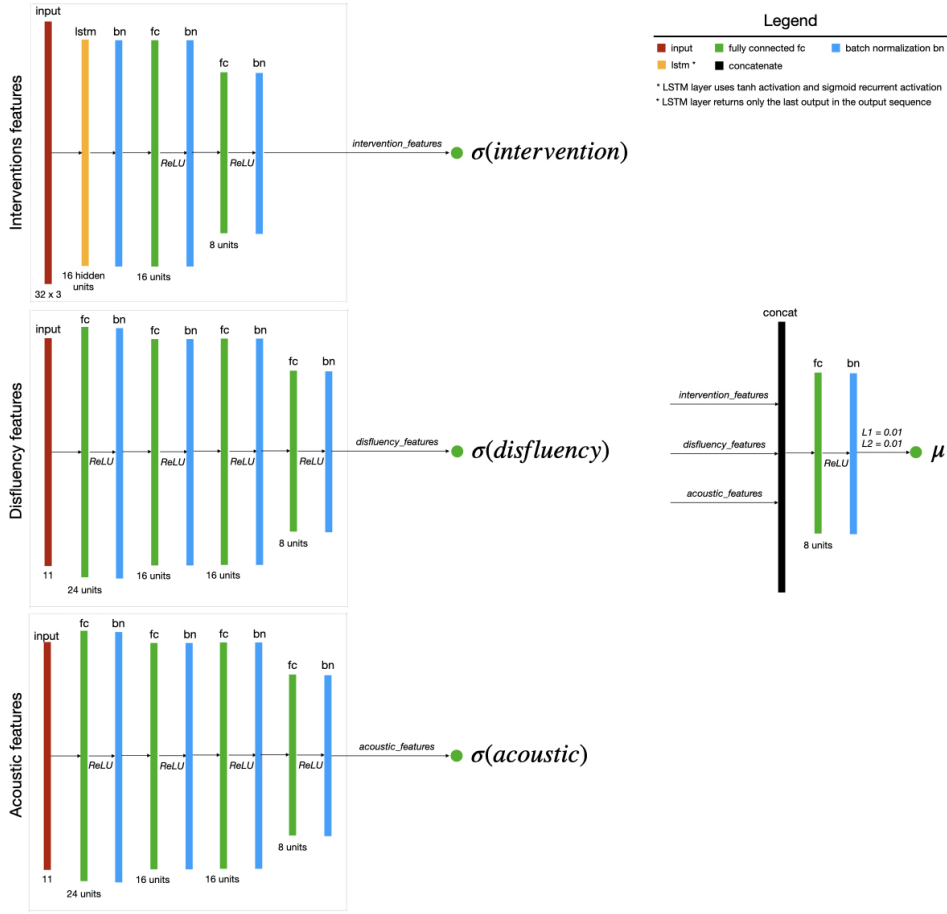


Figure 7: Model architecture of deep split NN for the ADReSS dataset.

Datasets	VI	PBP	MC Dropout	SI	RIO	Deep Ensembles	Anchored Ensembling	Deep Split Ensembles
Boston	4.32 ± 0.29	3.01 ± 0.18	2.97 ± 0.85	3.45 ± 0.95	–	3.28 ± 1.00	3.09 ± 0.17	<b>2.53 ± 0.15</b>
Concrete	7.13 ± 0.12	5.67 ± 0.09	5.23 ± 0.53	5.19 ± 0.44	5.97 ± 0.48	6.03 ± 0.58	4.87 ± 0.11	<b>4.40 ± 0.10</b>
Energy	2.65 ± 0.08	1.80 ± 0.05	1.66 ± 0.19	1.59 ± 0.27	0.70 ± 0.38	2.09 ± 0.29	<b>0.35 ± 0.01</b>	0.41 ± 0.02
Kin8nm	0.10 ± 0.00	0.10 ± 0.00	0.10 ± 0.00	–	–	0.09 ± 0.00	<b>0.07 ± 0.00</b>	0.19 ± 0.00
Naval	0.01 ± 0.00	0.01 ± 0.00	0.01 ± 0.00	<b>0.00 ± 0.00</b>	–	<b>0.00 ± 0.00</b>	<b>0.00 ± 0.00</b>	<b>0.00 ± 0.00</b>
Power	4.32 ± 0.04	4.12 ± 0.03	<b>4.02 ± 0.18</b>	–	4.05 ± 0.12	4.11 ± 0.17	4.07 ± 0.04	4.04 ± 0.05
Protein	4.84 ± 0.03	4.73 ± 0.01	4.36 ± 0.04	–	4.08 ± 0.06	4.71 ± 0.06	4.36 ± 0.02	<b>4.05 ± 0.03</b>
Wine	0.65 ± 0.01	0.64 ± 0.01	0.62 ± 0.04	–	0.67 ± 0.03	0.64 ± 0.04	0.63 ± 0.01	<b>0.60 ± 0.02</b>
Yacht	6.89 ± 0.67	1.02 ± 0.05	1.11 ± 0.38	0.97 ± 0.37	1.46 ± 0.49	1.58 ± 0.48	<b>0.57 ± 0.05</b>	0.86 ± 0.07

Table 10: Results on UCI regression datasets comparing RMSE<sup>6</sup>

## E.2 65-95-99.7 rule (empirical rule) to assess calibration

We evaluate to obtain calibration curves, where first, we compute the  $x\%$  prediction interval for each test datapoint based on Gaussian quantiles using the predicted mean and variance. Then, we calculate the fraction of test observations (true values) that fall within this prediction interval. For a

well-calibrated model, the observed fraction should be close to  $x\%$  calculated earlier. To see how our models perform in this setting, we sweep from  $x = 10\%$  to  $x = 90\%$  in steps of 10, and consequently a line lying very close to the line ( $y = x$ ) would indicate a well-calibrated model. Figure 10 shows the calibration curves for each feature cluster of DEPC, AEPC, and deep split ensembles on UCI datasets.

<sup>6</sup>RMSE values for dVI are not shown as they were not reported in the paper.

Datasets	VI	PBP	MC Dropout	dVI	SI	RIO	Deep Ensembles	Anchored Ensembling	Deep Split Ensembles
Boston	2.90±0.07	2.57±0.09	2.46±0.25	2.41±0.02	2.71±0.13	–	2.41±0.25	2.52±0.05	<b>2.23±0.04</b>
Concrete	3.39±0.02	3.16±0.02	3.04±0.09	3.06±0.01	3.00±0.08	3.24±0.10	3.06±0.18	2.97±0.02	<b>2.85±0.02</b>
Energy	2.39±0.03	2.04±0.02	1.99±0.09	1.01±0.06	1.56±1.24	1.03±0.35	1.38±0.22	0.96±0.13	<b>0.28±0.11</b>
Kin8nm	-0.90±0.01	-0.90±0.01	-0.95±0.03	-1.13±0.00	–	–	<b>-1.20±0.02</b>	-1.09±0.01	-0.20±0.02
Naval	-3.73±0.12	-3.73±0.01	-3.80±0.05	-6.29±0.04	-6.54±0.09	–	-5.63±0.05	<b>-7.17±0.03</b>	-5.28±0.02
Power	2.89±0.01	2.84±0.01	2.80±0.05	2.80±0.00	–	2.81±0.03	2.79±0.04	2.83±0.01	<b>2.78±0.01</b>
Protein	2.99±0.01	2.97±0.00	2.89±0.01	2.85±0.01	–	2.82±0.01	2.83±0.02	2.89±0.01	<b>2.76±0.00</b>
Wine	0.98±0.01	0.97±0.01	0.93±0.06	0.90±0.01	–	1.09±0.10	0.94±0.12	0.95±0.01	<b>0.89±0.02</b>
Yacht	3.44±0.16	1.63±0.02	1.55±0.12	0.47±0.03	0.225±0.40	1.79±0.88	1.18±0.21	<b>0.37±0.08</b>	0.90±0.09

Table 11: Results on UCI regression datasets comparing NLL

Datasets	RMSE			NLL		
	$E = 1$	$E = 5$	$E = 10$	$E = 1$	$E = 5$	$E = 10$
Boston	2.76 ± 1.16	<b>2.53 ± 0.15</b>	2.60 ± 1.31	2.33 ± 0.26	<b>2.23 ± 0.04</b>	2.25 ± 0.28
Concrete	4.52 ± 0.55	<b>4.40 ± 0.10</b>	4.63 ± 0.57	2.89 ± 0.12	<b>2.85 ± 0.02</b>	2.87 ± 0.13
Energy	0.43 ± 0.06	<b>0.41 ± 0.02</b>	0.44 ± 0.08	0.31 ± 0.19	<b>0.28 ± 0.11</b>	0.33 ± 0.25
Kin8nm	0.20 ± 0.00	<b>0.19 ± 0.00</b>	<b>0.19 ± 0.00</b>	-0.18 ± 0.03	<b>-0.20 ± 0.02</b>	<b>-0.20 ± 0.02</b>
Naval	<b>0.00 ± 0.00</b>	<b>0.00 ± 0.00</b>	<b>0.00 ± 0.00</b>	-5.21 ± 0.07	<b>-5.28 ± 0.02</b>	-5.26 ± 0.03
Power	4.06 ± 0.25	<b>4.04 ± 0.05</b>	4.07 ± 0.26	2.80 ± 0.05	<b>2.78 ± 0.01</b>	2.83 ± 0.06
Protein	4.14 ± 0.03	<b>4.05 ± 0.03</b>	4.09 ± 0.04	2.79 ± 0.01	<b>2.76 ± 0.00</b>	2.80 ± 0.02
Wine	0.63 ± 0.12	<b>0.60 ± 0.02</b>	<b>0.60 ± 0.05</b>	0.95 ± 0.17	<b>0.89 ± 0.02</b>	0.92 ± 0.10
Yacht	0.89 ± 0.41	<b>0.86 ± 0.07</b>	0.90 ± 0.46	0.93 ± 0.25	<b>0.90 ± 0.09</b>	0.93 ± 0.20

Table 12: Results of deep split ensembles with different no. of models  $E$  in the parallel ensemble.

Dataset	Cluster	Cluster-wise NLL		
		$E = 1$	$E = 5$	$E = 10$
Boston	1	$2.29 \pm 0.07$	$2.23 \pm 0.04$	<b><math>2.21 \pm 0.03</math></b>
	2	$2.33 \pm 0.08$	<b><math>2.20 \pm 0.05</math></b>	$2.24 \pm 0.03$
	3	$2.37 \pm 0.03$	<b><math>2.26 \pm 0.04</math></b>	$2.30 \pm 0.05$
Concrete	1	$2.87 \pm 0.01$	<b><math>2.84 \pm 0.02</math></b>	$2.87 \pm 0.03$
	2	$2.89 \pm 0.02$	<b><math>2.85 \pm 0.02</math></b>	$2.91 \pm 0.04$
	3	$2.91 \pm 0.03$	<b><math>2.87 \pm 0.01</math></b>	$2.93 \pm 0.02$
Energy	1	$0.28 \pm 0.20$	<b><math>0.26 \pm 0.11</math></b>	$0.29 \pm 0.27$
	2	$0.34 \pm 0.18$	<b><math>0.30 \pm 0.11</math></b>	$0.37 \pm 0.24$
Kin8nm	1	$-0.18 \pm 0.03$	$-0.19 \pm 0.02$	<b><math>-0.20 \pm 0.02</math></b>
	2	$-0.18 \pm 0.03$	$-0.19 \pm 0.03$	<b><math>-0.20 \pm 0.02</math></b>
	3	$-0.18 \pm 0.03$	$-0.19 \pm 0.02$	<b><math>-0.20 \pm 0.03</math></b>
	4	$-0.18 \pm 0.03$	$-0.19 \pm 0.03$	<b><math>-0.20 \pm 0.02</math></b>
	5	$-0.18 \pm 0.03$	<b><math>-0.20 \pm 0.03</math></b>	<b><math>-0.20 \pm 0.02</math></b>
	6	$-0.18 \pm 0.03$	$-0.19 \pm 0.02$	<b><math>-0.20 \pm 0.02</math></b>
	7	$-0.18 \pm 0.02$	<b><math>-0.20 \pm 0.03</math></b>	<b><math>-0.20 \pm 0.02</math></b>
	8	$-0.18 \pm 0.02$	<b><math>-0.21 \pm 0.02</math></b>	<b><math>-0.21 \pm 0.02</math></b>
Naval	1	$-5.19 \pm 0.08$	<b><math>-5.25 \pm 0.02</math></b>	$-5.23 \pm 0.04$
	2	$-5.24 \pm 0.06$	<b><math>-5.31 \pm 0.02</math></b>	$-5.29 \pm 0.02$
Power	1	$2.80 \pm 0.06$	<b><math>2.79 \pm 0.01</math></b>	$2.83 \pm 0.07$
	2	$2.81 \pm 0.05$	<b><math>2.80 \pm 0.01</math></b>	$2.84 \pm 0.05$
Protein	1	$2.73 \pm 0.01$	<b><math>2.68 \pm 0.01</math></b>	$2.72 \pm 0.02$
	2	$2.83 \pm 0.00$	<b><math>2.80 \pm 0.00</math></b>	$2.84 \pm 0.01$
	3	$2.83 \pm 0.00$	<b><math>2.81 \pm 0.00</math></b>	$2.86 \pm 0.02$
Wine	1	$0.95 \pm 0.05$	<b><math>0.91 \pm 0.03</math></b>	$0.94 \pm 0.03$
	2	$0.99 \pm 0.08$	<b><math>0.92 \pm 0.01</math></b>	<b><math>0.92 \pm 0.08</math></b>
	3	$0.94 \pm 0.04$	<b><math>0.91 \pm 0.02</math></b>	<b><math>0.91 \pm 0.08</math></b>
	4	$0.94 \pm 0.05$	<b><math>0.90 \pm 0.04</math></b>	$0.94 \pm 0.03$
	5	$0.95 \pm 0.07$	<b><math>0.91 \pm 0.01</math></b>	<b><math>0.91 \pm 0.08</math></b>
Yacht	1	$1.48 \pm 0.20$	<b><math>1.45 \pm 0.10</math></b>	$1.49 \pm 0.12$
	2	$0.39 \pm 0.10$	<b><math>0.36 \pm 0.09</math></b>	$0.38 \pm 0.08$

Table 13: NLLs of all clusters for different number of models  $E$  in the parallel ensemble.

Datasets	RMSE			Clusters	Cluster-wise NLL		
	DEPC	AEPC	Deep Split Ens.		DEPC	AEPC	Deep Split Ens.
Boston	$5.11 \pm 1.06$	$4.93 \pm 1.03$	<b><math>2.53 \pm 0.15</math></b>	1	$2.91 \pm 0.16$	$3.87 \pm 0.82$	$2.23 \pm 0.04$
				2	$2.82 \pm 0.16$	$3.99 \pm 0.94$	$2.20 \pm 0.05$
				3	$3.29 \pm 0.10$	$4.23 \pm 1.06$	$2.26 \pm 0.04$
Concrete	$10.22 \pm 0.82$	$10.40 \pm 0.93$	<b><math>4.40 \pm 0.10</math></b>	1	$3.77 \pm 0.05$	$5.75 \pm 0.61$	$2.84 \pm 0.02$
				2	$3.79 \pm 0.10$	$5.68 \pm 0.60$	$2.85 \pm 0.02$
				3	$3.81 \pm 0.05$	$5.83 \pm 0.61$	$2.87 \pm 0.01$
Power	$7.51 \pm 0.20$	$7.53 \pm 0.18$	<b><math>4.04 \pm 0.05</math></b>	1	$3.90 \pm 0.09$	$4.20 \pm 0.09$	$2.79 \pm 0.01$
				2	$3.61 \pm 0.02$	$4.18 \pm 0.09$	$2.80 \pm 0.01$
Protein	$5.04 \pm 0.01$	$5.00 \pm 0.02$	<b><math>4.05 \pm 0.03</math></b>	1	$3.83 \pm 0.10$	$3.04 \pm 0.00$	$2.68 \pm 0.01$
				2	$3.04 \pm 0.00$	$3.05 \pm 0.00$	$2.80 \pm 0.00$
				3	$3.06 \pm 0.00$	$3.05 \pm 0.00$	$2.81 \pm 0.00$
Wine	$0.67 \pm 0.05$	$0.69 \pm 0.04$	<b><math>0.60 \pm 0.02</math></b>	1	$1.02 \pm 0.07$	$1.08 \pm 0.10$	$0.91 \pm 0.03$
				2	$1.01 \pm 0.06$	$1.08 \pm 0.09$	$0.92 \pm 0.01$
				3	$1.01 \pm 0.06$	$1.08 \pm 0.09$	$0.91 \pm 0.02$
				4	$1.01 \pm 0.06$	$1.09 \pm 0.09$	$0.90 \pm 0.04$
				5	$0.99 \pm 0.07$	$1.09 \pm 0.09$	$0.91 \pm 0.01$

Table 14: RMSE and Cluster-wise NLL values for DEPC, AEPC, DSE on UCI datasets



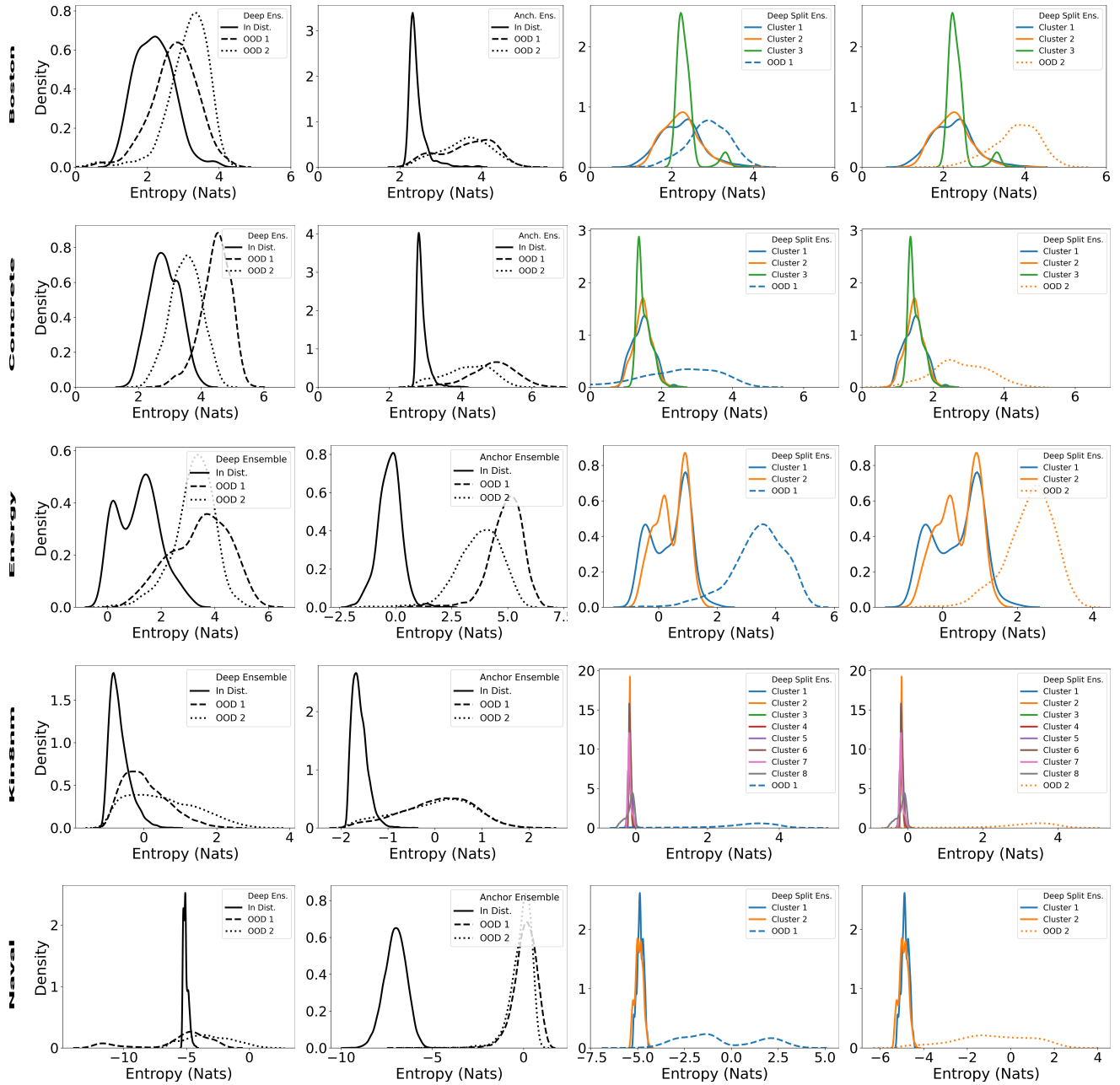


Figure 8: Entropy plots for ‘Boston’, ‘Concrete’, ‘Energy’, ‘Kin8nm’, and ‘Naval’ datasets using hierarchical clustering (Section 2.3). The first two columns show the kernel density estimation (KDE) of entropy for in- distribution i.e.  $\mathcal{N}(0, 1)$  and out-of-distribution samples, obtained with unified uncertainty estimation using deep ensemble and anchored ensembling respectively. The last two columns show ‘cluster-wise’ KDE of entropy for in-distribution and out-of-distribution samples, obtained with disentangled uncertainty estimation using deep split ensembles. OOD 1 and OOD 2 refer to introducing dataset shift by inducing noise sampled from  $\mathcal{N}(6, 2^2)$  into 2 random input features; the features correspond to different clusters for deep split ensembles.

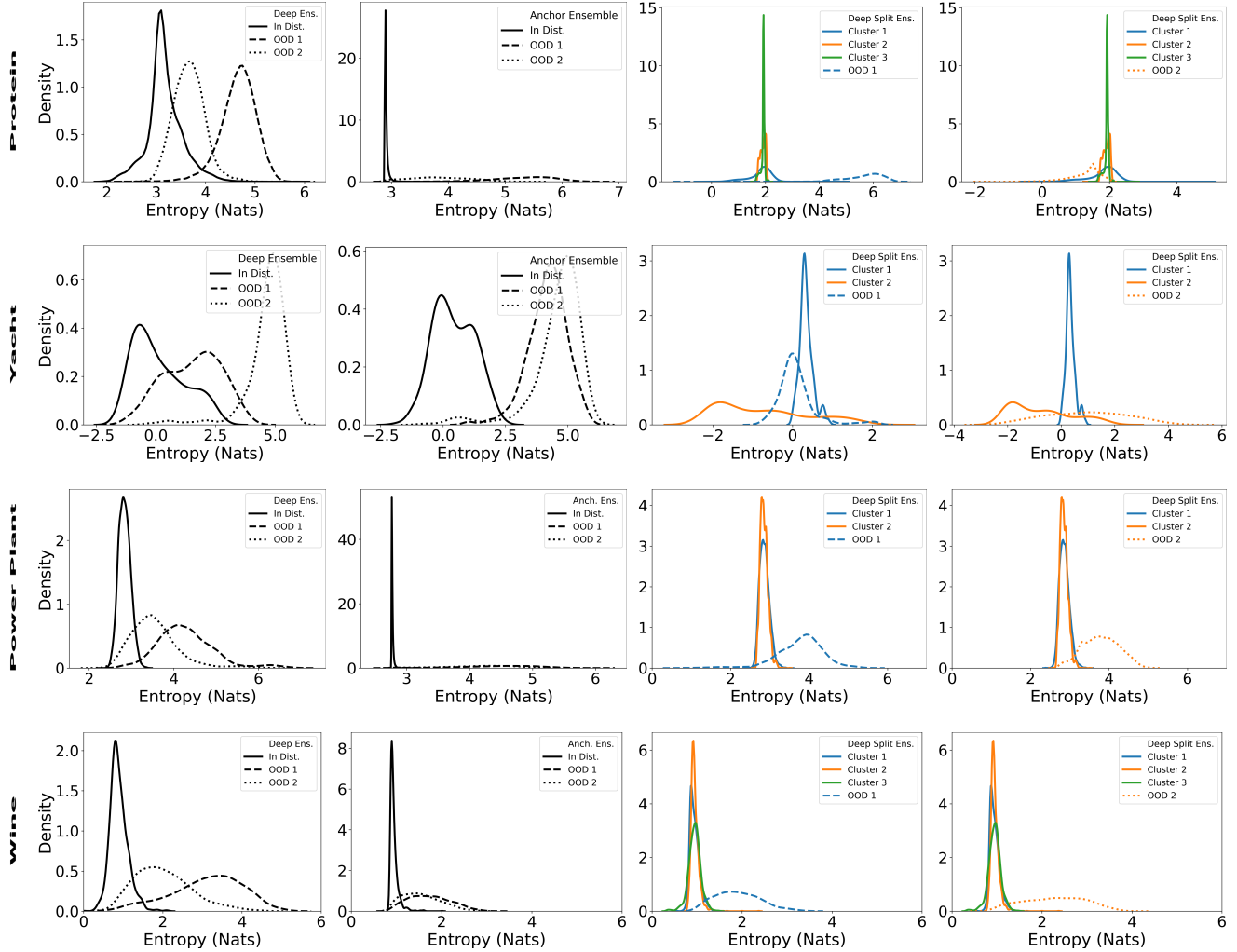


Figure 9: Entropy plots for 'Protein' and 'Yacht' datasets using hierarchical clustering (Section 2.3), and 'Power Plant' and 'Wine' datasets using clusters from human experts (Section 3.4). The first two columns show the kernel density estimation (KDE) of entropy for in- distribution i.e.  $\mathcal{N}(0, 1)$  and out-of-distribution samples, obtained with unified uncertainty estimation using deep ensemble and anchored ensembling respectively. The last two columns show 'cluster-wise' KDE of entropy for in-distribution and out-of-distribution samples, obtained with disentangled uncertainty estimation using deep split ensembles. OOD 1 and OOD 2 refer to introducing dataset shift by inducing noise sampled from  $\mathcal{N}(6, 2^2)$  into 2 random input features; the features correspond to different clusters for deep split ensembles.

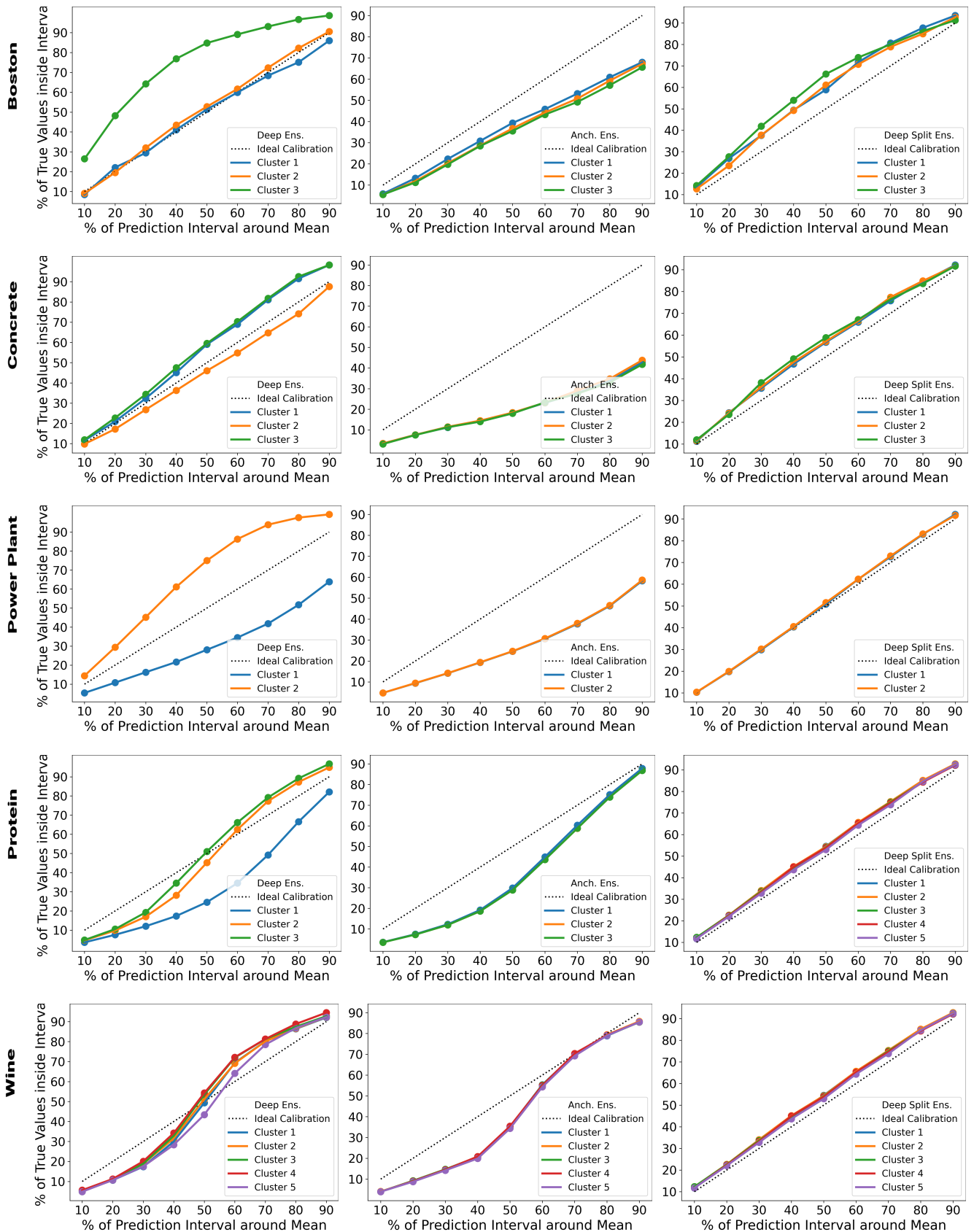


Figure 10: ‘Cluster-wise’ calibration curves using empirical rule for ‘Boston’, ‘Concrete’, ‘Power’, ‘Protein’, and ‘Wine’ datasets using hierarchical clustering (Section 2.3). The columns contain experiments using deep ensemble per input cluster (DEPC), anchored ensembling per input cluster (AEPC) and deep split ensembles respectively.